DTD 5

ARTICLE IN PRESS

Available online at www.sciencedirect.com

SCIENCE DIRECT®

ELSEVIER

Sensors and Actuators A xxx (2005) xxx–xxx

SENSORS AND ACTUATORS A PHYSICAL

www.elsevier.com/locate/sna

Influence of electromagnetic interferences on the mass sensitivity of Love mode surface acoustic wave sensors

Laurent A. Francis[a,b,*], Jean-Michel Friedt[c], Patrick Bertrand[a]

[a] PCPM, Université catholique de Louvain, Croix du Sud 1, B-1348 Louvain-la-Neuve, Belgium
[b] IMEC, Kapeldreef 75, B-3001 Leuven, Belgium
[c] LPMO, Université de Franche-Comté, La Bouloie, 25030 Besançon, France

Received 13 September 2004; received in revised form 2 March 2005; accepted 3 March 2005

Abstract

Surface acoustic waveguides have found an application for (bio)chemical detection. The mass modification due to surface adsorption leads to measurable changes in the propagation properties of the waveguide. Among a wide variety of waveguides, the Love mode device has been investigated because of its high mass sensitivity. The acoustic signal launched and detected in the waveguide by electrical transducers is accompanied by an electromagnetic wave; the interaction of the two signals, easily enhanced by the open structure of the sensor, creates interference patterns in the transfer function of the sensor. The interference peaks are used to determine the sensitivity of the acoustic device. We show that electromagnetic interferences generate a distortion in the experimental value of the sensitivity. This distortion is not identical for the two classical instrumentation of the sensor that are the open and the closed loop configurations. Our theoretical approach is completed by the experimentation of an actual Love mode sensor operated under liquid conditions and in an open loop configuration. The experiment indicates that the interaction depends on frequency and mass modifications.
© 2004 Published by Elsevier B.V.

Keywords: Surface acoustic wave; Electromagnetic wave; Love mode; Interferences; Gravimetric sensitivity; Biosensor

1. Introduction

Acoustic waves guided by the surface of solid structures form waveguides used as delay lines and filters in telecommunications [1]. Waveguides support different modes with specific strain and stress fields [2]. The acoustic velocity of each mode depends on different intrinsic and extrinsic parameters such as the mechanical properties of the materials, the temperature or the applied pressure. Waveguides are used as sensors when the velocity change is linked to environmental changes. For gravimetric sensors, the outer surface of the waveguide is exposed to mass changes. Due to the confinement of the acoustic wave energy close to the surface, these sensors are well suited for (bio)chemical sensors operating in gas or liquid media. Among a wide variety of waveguides used for that purpose, Love mode sensors have attracted an increasing interest during the last decade [3,4]. A Love mode is guided by a solid overlayer deposited on top of a substrate material. The usual substrates are piezoelectric materials like quartz, lithium tantalate and lithium niobate [5]. Associated to specific crystal cut of these substrates, the Love mode presents a shear-horizontal polarization that makes it suitable for sensing in liquid media.

Current research in Love mode sensors concerns the guiding materials in order to optimize the sensitivity, that is the variation of the acoustic signal under surface modifications. Typical materials under investigations are dielectrics like silicon dioxide and polymers, and more recently semiconductors with piezoelectric properties like zinc oxide [6–8]. Although the dispersion relation for Love mode is well set and the dependence of the sensitivity of the liquid loaded sensor to the overlayer thickness has been thoroughly investigated [9–11], little has been devoted to study the role played by the structure of the sensor and their transducers.

* Corresponding author. Tel.: +32 16 281211; fax: +32 16 229400.
E-mail address: francisl@ieee.org (L.A. Francis).

0924-4247/$ – see front matter © 2004 Published by Elsevier B.V.
doi:10.1016/j.sna.2005.03.030

UNCORRECTED PROOF

In this paper, we investigate the role played by the structure of the sensor and by the interferences between the acoustic and the electromagnetic waves on the sensitivity. In the first part, we present a general model of the transfer function including the influence of electromagnetic interferences. In the second part, we show how these interferences modify the sensitivity in open and closed loop configurations of the sensor. Finally, these effects are illustrated experimentally on a Love mode sensor.

2. Modeling

Waveguide sensors consist of a transducing part and a sensing part. The transducing part includes the generation and the reception of acoustic signals and their interfacing to an electrical instrumentation. The most common transducers are the widespread interdigital transducers (IDTs) on piezoelectric substrates introduced by White and Voltmer in 1965 [12]. Although the transducing part can be involved in the sensing part, practical sensing is confined to the spacing between the transducers. This confinement takes especially place when liquids are involved since these produce large and unwanted capacitive coupling between input and output electrical transducers. This coupling dramatically deteriorates the transfer function and is an important issue for the instrumentation and the packaging of the sensors.

The sensor itself is configured as a delay line formed by two transducers separated by a certain distance. The sensor can also be configured as a resonator but we will restrict our approach to the delay line configuration because the operation principle in these two configurations is not similar. The Love mode sensor is sketched in Fig. 1. Transducers with a constant apodization are identified to their midpoint; the distance between the midpoints is L and the interdigitated electrodes have a periodicity λ_T. The sensing part is located between the transducers and covers a total length D so that $D \leq L$. The guided mode propagates with a phase velocity $V = \omega/k$, where $\omega = 2\pi f$ is the angular frequency and $k = 2\pi/\lambda$ is the wavenumber. The waveguide is dispersive when the group velocity ($V_g = \mathrm{d}\omega/\mathrm{d}k$) differs from the phase velocity.

The velocity is a function of the frequency and of the surface density $\sigma = M/A$ for a rigidly bound and non viscous mass M per surface area A. For an uniformly distributed mass, the surface density is rewritten in terms of material density ρ and thickness d by $\sigma = \rho d$. The phase velocity for an initial and constant mass σ_0 is denoted V_0, and the group velocity V_{g0}. In the sensing part, the phase velocity is V and the group velocity V_g. According to this model, the transit time τ on the delay line is given by

$$\tau = \frac{D}{V} + \frac{L-D}{V_0}. \tag{1}$$

Electromagnetic interferences are due to the cross-talk between the IDTs [13]. The electromagnetic wave (EM) emitted by the input transducer travels much faster than the acoustic wave and therefore is detected at the output transducer without noticeable delay. At the output transducer, the two kinds of waves interact with an amplitude ratio, denoted by α, that creates interference patterns in the transfer function $H(\omega)$ of the delay line. The transfer function itself is given by the ratio of the output to the input voltages. The transfer function with electromagnetic interferences is modeled by the following equation:

$$H(\omega) = \underbrace{H_T(\omega)\exp(-\mathrm{i}\omega\tau)}_{\text{delay line}} + \underbrace{\alpha H_T(\omega)}_{\text{EM coupling}}. \tag{2}$$

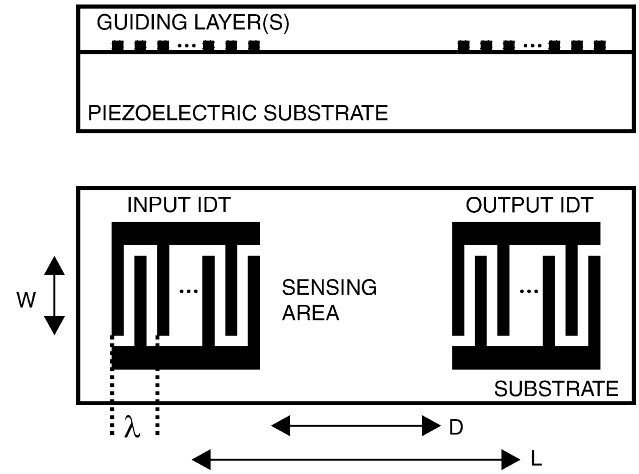

Fig. 1. Structure of the acoustic device.

The transfer function $H_T(\omega)$ is associated to the design of the transducers. The total transfer function can be rewritten as $H(\omega) = \|H(\omega)\| \exp(\mathrm{i}\phi)$ where expressions for the amplitude $\|H(\omega)\|$ and the phase ϕ are obtained with help of complex algebra:

$$\|H(\omega)\| = \|H_T(\omega)\| \|\sqrt{1 + 2\alpha\cos(\omega\tau) + \alpha^2}\|; \tag{3}$$

$$\phi = \phi_0 - \arctan\left(\frac{\sin(\omega\tau)}{\alpha + \cos(\omega\tau)}\right). \tag{4}$$

The phase ϕ_0 corresponds to the packaging of the sensor and is due to different aspects linked to the instrumentation. It will be assumed independent of the frequency and of the sensing event. The synchronous frequency $\omega_T = 2\pi f_T$ is determined by the design of the IDTs and is generally equal to the maximum amplitude of $\|H_T(\omega)\|$ when the wavelength of the acoustic wave λ_0 matches the transducers periodicity λ_T.

The relations (3) and (4) are the sources of ripples in the transfer function at the ripple frequency $\Delta\omega \simeq 2\pi/\tau$, its exact expression depends also of the dispersion on the line. Interference peaks corresponding to the maximum effect are observed at quantified frequencies f_n when $\cos(2\pi f_n\tau) = -1$, that is for frequencies such that

$$f_n = \frac{2n+1}{2\tau} \tag{5}$$

UNCORRECTED PROOF

where $n \in \mathbb{N}$ is the interference mode number. A direct relation to the velocity in the sensing area is obtained from this latter equation as seen by replacing the transit time τ by its definition:

$$V = \frac{2DV_0 f_n}{(2n+1)V_0 + 2(D-L)f_n}. \tag{6}$$

The interference mode numbers are determined by considering the uncovered delay line; in such case $V = V_0$ and $D = L$, and n for the interference peak located below the synchronous frequency (i.e. for $f_n \leq f_\mathrm{T}$) is given by

$$n = \left\lfloor \frac{L}{\lambda_\mathrm{T}} - \frac{1}{2} \right\rfloor \tag{7}$$

while the other peaks are labeled subsequently to their position with respect to the peak referenced by Eq. (7).

The relative amplitude peak to peak of the perturbation on the amplitude has a maximum effect (in dB) equals to $40\log[(1+\alpha)/(1-\alpha)]$. The amplitude (in dB and normalized to have $\|H_\mathrm{T}(\omega)\| = 1$) and the phase (in radians) as a function of the frequency are simulated in Figs. 2–5 for different values of α.

Under the influence of the interferences, the phase has different behaviors function of α:

(1) when $\alpha = 0$ (no interferences), the phase is linear with the frequency and has a periodicity equal to 2π (Fig. 2);
(2) when $\alpha < 1$, the phase is deformed but has still a periodicity equal to 2π (Fig. 3);
(3) when $\alpha = 1$, the phase has a periodicity equal to π (Fig. 4);
(4) when $\alpha > 1$, the periodicity is lower than π (Fig. 5);
(5) when $\alpha \to \infty$, the phase is not periodic anymore and its value tends to ϕ_0.

This specific behavior of the phase under the influence of the electromagnetic interferences has to be considered while evaluating the sensitivity.

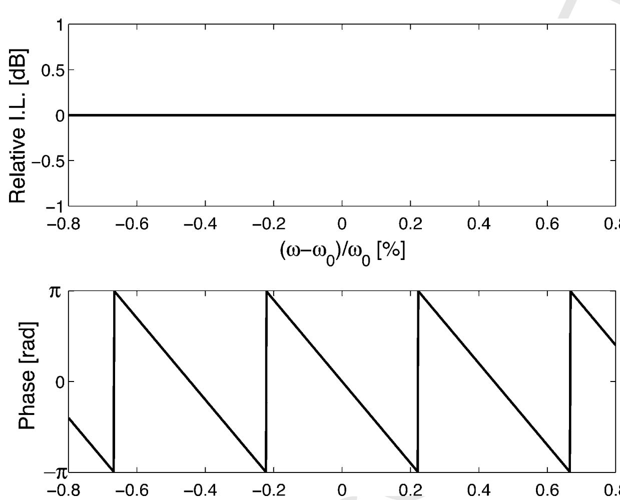

Fig. 2. Relative insertion loss (top) and phase (bottom) of the transfer function for $\alpha = 0$.

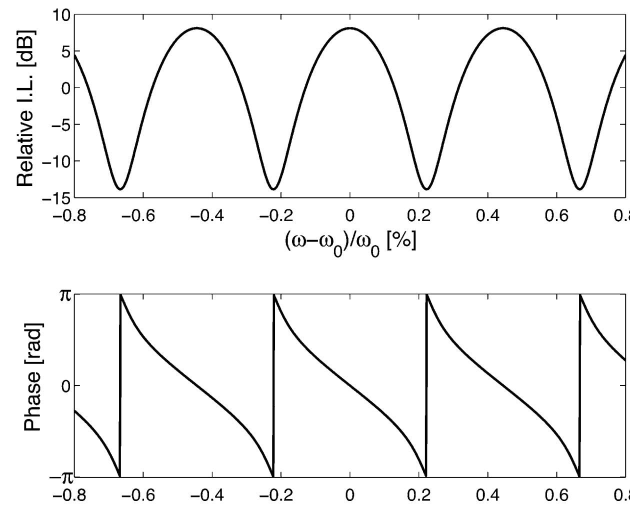

Fig. 3. Relative insertion loss (top) and phase (bottom) of the transfer function for $\alpha = 1/2$.

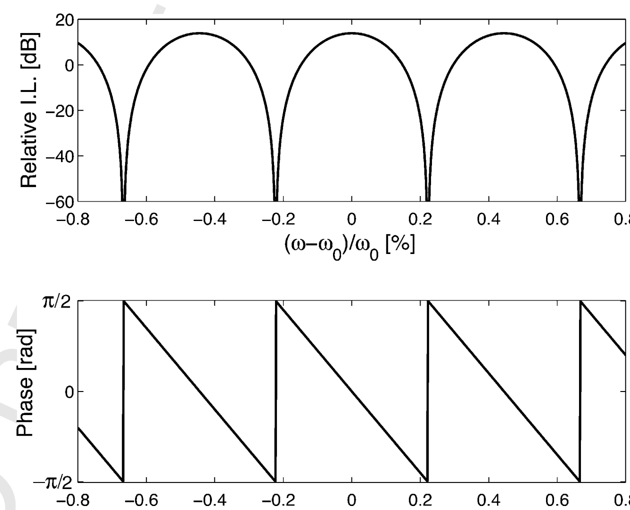

Fig. 4. Relative insertion loss (top) and phase (bottom) of the transfer function for $\alpha = 1$.

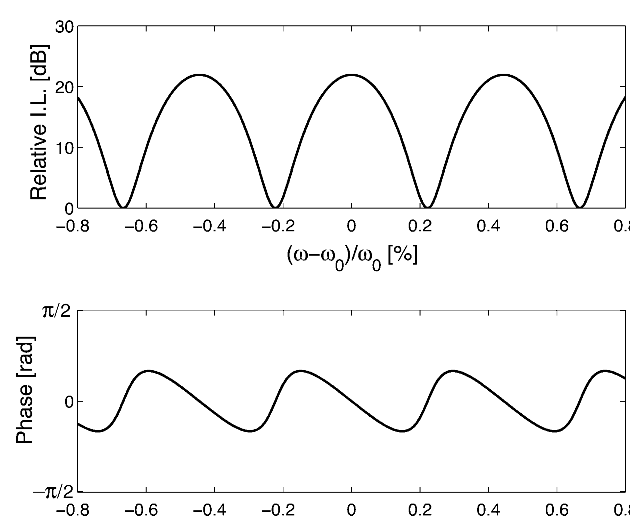

Fig. 5. Relative insertion loss (top) and phase (bottom) of the transfer function for $\alpha = 2$.

3. Sensitivity

Changes in the boundary condition of the waveguide due to the sensing event modify phase and group velocities. As consequence, the transit time of the delay line and the phase of the transfer function are modified. The sensing event is quantified by recording the phase shift at a fixed frequency (open loop configuration) or the frequency shift at a fixed phase (closed loop configuration). This quantification gives rise to the concept of sensitivity. The sensitivity is not an unique concept for acoustic sensors because various parameters influence the acoustic velocity. As example of such parameters, there is the density and the viscosity of liquid solutions and adsorbed biomolecules film when the device is used as biosensor. The sensitivity is the most important parameter in design, calibration and applications of acoustic waveguide sensors. Its measurement must be carefully addressed in order to extract the intrinsic properties of the sensor.

3.1. Definitions of the sensitivity

The *velocity sensitivity* S_V is defined by the change of phase velocity as a function of the surface density change at a constant frequency. Its mathematical expression is given by [10]:

$$S_V = \frac{1}{V}\frac{\partial V}{\partial \sigma}\bigg|_{\omega}. \tag{8}$$

The definition reflects the velocity change in the sensing area only while outside this area the velocity remains unmodified. The expression is general because the initial velocity V of the sensing part does not need to be equal to V_0; this situation occurs in practical situations where the sensing part has a selective coating with its own mechanical properties, leading to an initial difference between V and V_0.

To link the sensitivity (caused by the unknown velocity shift) to the experimental values of phase and frequency shifts, we introduce two additional definitions related to the open and the close loop configurations, respectively. The *phase sensitivity* S_ϕ is defined by

$$S_\phi = \frac{1}{kD}\frac{\mathrm{d}\phi}{\mathrm{d}\sigma}, \tag{9}$$

and the *frequency sensitivity* S_ω is defined by

$$S_\omega = \frac{1}{\omega}\frac{\mathrm{d}\omega}{\mathrm{d}\sigma}. \tag{10}$$

3.2. Phase differentials without interferences

In order to point clearly the effects of the electromagnetic interferences on the different sensitivities presented in the previous section, we calculate the phase differentials in the ideal case of no interferences. For that case, the phase of the transfer function is a function of the frequency and of the velocities in the different parts of the sensor, themselves function of the frequency and of the surface density:

$$\phi(\omega, V(\omega,\sigma), V_0(\omega)) = -\omega\tau \tag{11}$$

$$\phi(\omega, V(\omega,\sigma), V_0(\omega)) = -\omega\left(\frac{D}{V} + \frac{L-D}{V_0}\right). \tag{12}$$

Therefore, the total differential of the phase is

$$\mathrm{d}\phi = \left(\frac{\partial\phi}{\partial\omega}\bigg|_{V,V_0} + \frac{\partial\phi}{\partial V}\bigg|_{\omega,V_0}\frac{\partial V}{\partial\omega}\bigg|_{\sigma} + \frac{\partial\phi}{\partial V_0}\bigg|_{\omega,V}\frac{\mathrm{d}V_0}{\mathrm{d}\omega}\right)\mathrm{d}\omega + \frac{\partial\phi}{\partial V}\bigg|_{\omega,V_0}\frac{\partial V}{\partial\sigma}\bigg|_{\omega}\mathrm{d}\sigma \tag{13}$$

$$\mathrm{d}\phi = \frac{\partial\phi}{\partial\omega}\bigg|_{\sigma}\mathrm{d}\omega + \frac{\partial\phi}{\partial\sigma}\bigg|_{\omega}\mathrm{d}\sigma. \tag{14}$$

The derivative of the phase velocity as a function of the frequency comes from the definitions of phase and group velocities; at constant surface density, we have from [11]:

$$\frac{\partial V}{\partial\omega}\bigg|_{\sigma} = k^{-1}\left(1-\frac{V}{V_g}\right); \tag{15}$$

$$\frac{\mathrm{d}V_0}{\mathrm{d}\omega} = k_0^{-1}\left(1-\frac{V_0}{V_{g0}}\right). \tag{16}$$

The other partial differentials are obtained by differentiation of Eq. (11):

$$\frac{\partial\phi}{\partial\omega}\bigg|_{V,V_0} = -\tau; \tag{17}$$

$$\frac{\partial\phi}{\partial\omega}\bigg|_{\sigma} = -\tau - \omega\,\frac{\tau}{\omega}\bigg|_{\sigma} \tag{18}$$

$$\frac{\partial\phi}{\partial\omega}\bigg|_{\sigma} = -\tau_g; \tag{19}$$

$$\frac{\partial\phi}{\partial V}\bigg|_{\omega,V_0} = \frac{\omega D}{V^2}; \tag{20}$$

$$\frac{\partial\phi}{\partial V_0}\bigg|_{\omega,V} = \frac{\omega(L-D)}{V_0^2}. \tag{21}$$

The time of flight τ_g introduced in Eq. (19) is calculated as

$$\tau_g = \frac{D}{V_g} + \frac{L-D}{V_{g0}}. \tag{22}$$

3.3. Open loop configuration

In the open loop configuration, the input transducer is excited at a given frequency while the phase difference between output and input transducers is recorded. This configuration with a constant frequency has $\mathrm{d}\omega = 0$ in Eq. (13); related

UNCORRECTED PROOF

phase variations caused by surface density variations are obtained by

$$\frac{\mathrm{d}\phi}{\mathrm{d}\sigma}=\left.\frac{\partial\phi}{\partial V}\right|_{\omega,V_0}\left.\frac{\partial V}{\partial\sigma}\right|_{\omega} \tag{23}$$

$$\frac{\mathrm{d}\phi}{\mathrm{d}\sigma}=\left.\frac{\partial\phi}{\partial V}\right|_{\omega,V_0} VS_{\mathrm{V}}. \tag{24}$$

In the absence of interferences, phase variations obtained experimentally are directly linked to velocity changes by the product kD involving the geometry of the sensor as seen by replacing Eq. (20) in Eq. (24):

$$\frac{\mathrm{d}\phi}{\mathrm{d}\sigma}=kDS_{\mathrm{V}}. \tag{25}$$

In other words: $S_\phi=S_{\mathrm{V}}$ when there are no interferences. In a first approximation k is assumed equal to k_{T}, an assumption valid as long as the phase shift is evaluated close to the synchronous frequency and for waveguides with low dispersion. The wavelength is only known when the sensing part extends over the transducers ($D=L$). In that case, the transfer function of the IDTs is modified accordingly to the velocity changes. In practice, the value of the sensitivity is slightly underestimated to its exact value since $k\le k_{\mathrm{T}}$, the error being less than 5%.

In the case where interferences occur, the partial differential of ϕ with respect to the velocity is obtained by differentiation of Eq. (4):

$$\left.\frac{\partial\phi}{\partial V}\right|_{\omega,V_0}=\left(\frac{1+\alpha\,\cos(\omega\tau)}{1+2\alpha\,\cos(\omega\tau)+\alpha^2}\right)\frac{\omega D}{V^2}, \tag{26}$$

and the phase sensitivity is obtained by combining the latter equation with Eq. (24):

$$S_\phi=\left(\frac{1+\alpha\,\cos(\omega\tau)}{1+2\alpha\,\cos(\omega\tau)+\alpha^2}\right)S_{\mathrm{V}}. \tag{27}$$

The influence of electromagnetic interferences on the phase sensitivity is simulated in Fig. 6 versus the relative frequency for different values of α. The phase sensitivity is always different compared to the velocity sensitivity. For the threshold value $\alpha=1$, the phase sensitivity present a singularity and is undefined; for higher values of α, the phase sensitivity is always underestimated to the velocity sensitivity.

The interference peaks permit a direct evaluation of α because at these points $\cos(\omega\tau)=-1$ and Eq. (27) becomes linear with α:

$$\alpha=1-\frac{V^2}{\omega D}\left.\frac{\partial\phi}{\partial V}\right|_{\omega,V_0} \tag{28}$$

$$\alpha=1-\frac{S_{\mathrm{V}}}{S_\phi}. \tag{29}$$

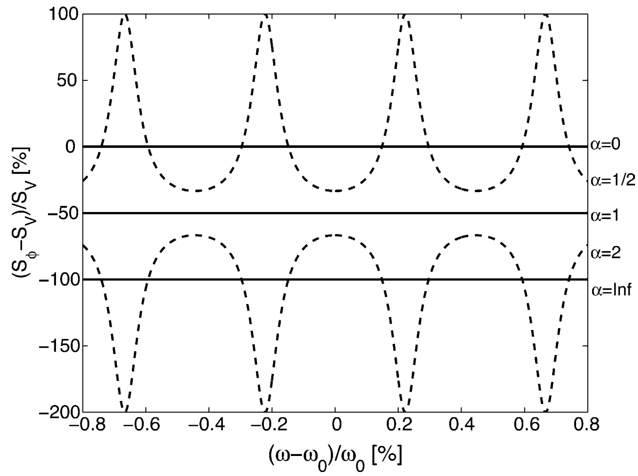

Fig. 6. Phase sensitivity at constant frequency as a function of the relative frequency for different values of simulated interferences obtained by Eq. (27).

3.4. Closed loop configuration

In the closed loop configuration, the frequency is recorded while a feedback loop keeps the phase difference between output and input transducers constant. The configuration at constant phase has $\mathrm{d}\phi=0$, the variation of the frequency as a function of the mass change is given by introducing this condition in Eq. (14):

$$\frac{\mathrm{d}\omega}{\mathrm{d}\sigma}=\left(\left.\frac{\partial\phi}{\partial\sigma}\right|_{\omega}\right)\left(\left.\frac{\partial\phi}{\partial\omega}\right|_{\sigma}\right)^{-1}. \tag{30}$$

The upper term is replaced by Eq. (24). The phase slope as a function of the frequency at constant mass is obtained by differentiation of Eq. (4):

$$\left.\frac{\partial\phi}{\partial\omega}\right|_{\sigma}=-\left(\frac{1+\alpha\,\cos(\omega\tau)}{1+2\alpha\,\cos(\omega\tau)+\alpha^2}\right)\tau_{\mathrm{g}}. \tag{31}$$

We can establish a finalized equation taking into account the electromagnetic interferences by combining Eqs. (24), (26) and (31) in Eq. (30):

$$S_\omega=\frac{DS_{\mathrm{V}}}{V\tau_{\mathrm{g}}}. \tag{32}$$

At the opposite of the open loop configuration, the frequency sensitivity is not influenced by the interferences. However, as indicated by Eq. (32), the frequency sensitivity is strongly dependent of the structure of the sensor and the dispersion characteristics of the delay line. As result, the link between the frequency sensitivity and the velocity sensitivity is difficult to exploit although it can be noticed that $S_\omega\le S_{\mathrm{V}}$ since $V_{\mathrm{g}}\le V$ for Love mode devices.

UNCORRECTED PROOF

4. Experimental results

For the practical consideration of the described and modeled behavior, we investigated a Love mode sensor. It was fabricated and tested under liquid condition in the open loop configuration to evaluate the influence of the electromagnetic interferences. In a first part, the sensor fabrication and instrumentation is described, followed in a second part by the application of the model to these results to demonstrate the influence of the interferences on the sensitivity of the sensor.

4.1. Sensor fabrication and instrumentation

The Love mode was obtained by conversion of a surface skimming bulk wave (SSBW) launched in the direction perpendicular to the crystalline X axis of a 500 μm thick ST-cut (42.5° Y-cut) quartz substrate. The conversion was achieved by a 1.2 μm thick overlayer of silicon dioxide deposited on the top side of the substrate by plasma enhanced chemical vapor deposition (Plasmalab 100 from Oxford Plasma Technology, England). Via were etched in the silicon dioxide layer using a standard SF_6/O_2 plasma etch recipe. This process stopped automatically on the aluminum contact pads of the transducers.

The transducers consist of split fingers electrodes etched in 200 nm thick sputtered aluminum. The fingers are 5 μm wide and equally spaced by 5 μm. This defines a periodicity λ_T of 40 μm. The acoustic aperture defined by the overlap of the fingers is equal to $80\lambda_T$ (=3.2 mm), the total length of each IDT is $100\lambda_T$ (=4 mm) and the distance center to center of the IDTs is $225\lambda_T$ ($L = 9$ mm, $D = 5$ mm).

The sensing area was defined by covering the space left between the edges of the IDTs by successive evaporation and lift-off of 10 nm of titanium and 50 nm of gold in a first experiment, and 200 nm of gold in a second experiment. The fingers were protected against liquid by patterning photosensitive epoxy SU-8 2075 (Microchem Corp., MA) defining 120 μm thick and 80 μm wide walls around the IDTs. Quartz glasses of 5 mm × 5 mm were glued on top of the walls to finalize the protection of the IDTs [14].

The device was mounted and wire-bonded to an epoxy printed circuit board and its transfer function was recorded on a HP4396A Network Analyzer. This setup corresponds to the open loop configuration. Epoxy around the device covered and protected it and defined a leak-free liquid cell. The sensing area was immersed in a solution of KI/I_2 (4 and 1 g, respectively, in 160 ml of water) that etched the gold away of the surface [15]. The transfer function of the device was recorded every 4 s (limited by the GPIB transfer speed) during the etching of the gold with a resolution of 801 points over a span of 2 MHz centered around 123.5 MHz. The initial transfer function of the device is presented in Fig. 7 with and without gold. The transfer function during etching of the 200 nm is shown at two moments (44 and 356 s after etching start) in Fig. 8. The total time for this etching was approximately 620 s.

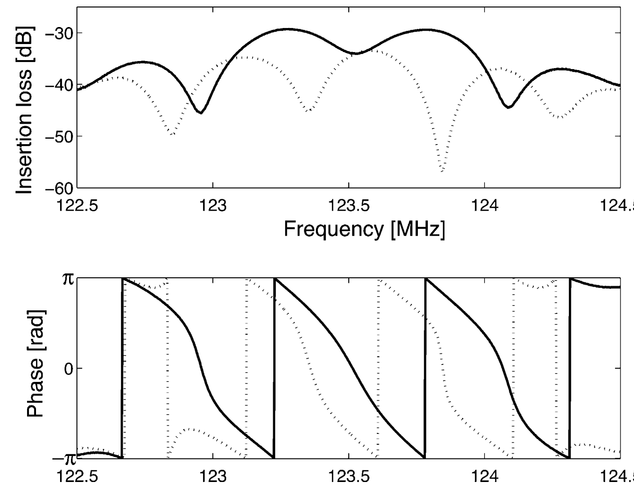

Fig. 7. Initial aspect of the experimentally recorded transfer function of the Love mode sensor with (dashed line) and without (solid line) an overlayer of 200 nm of gold. This device presents an initial phase $\phi_0 = \pi$, leading to a vertical offset by π compared to the simulated phase curve represented in Fig. 3.

4.2. Correlation of the results with the model

The correlation of the experimental results with the model is presented in two steps. In the first step, we show the calculation of the phase velocity from the interference peaks; and in the second step, we evaluate the mass sensitivity in the open loop configuration by the delay phase angle and the phase velocity variations recorded during the gold etching.

The record of the interference peaks frequency f_n during a sensing event permits to follow the evolution of the phase velocity in the sensing area either for constant and integer values of the interference mode numbers n as given by Eq. (6),

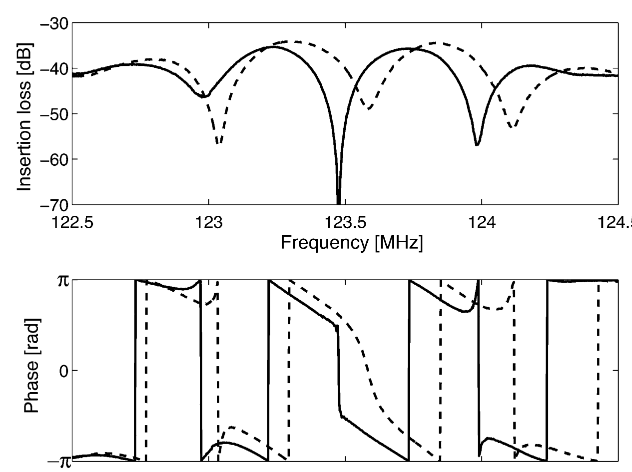

Fig. 8. Aspect of the experimentally recorded transfer function at two different moments of the etching of 200 nm of gold (solid line after 44 s and dashed line after 356 s). The solid line shows a value of α close to 1 around 123.5 MHz.

UNCORRECTED PROOF

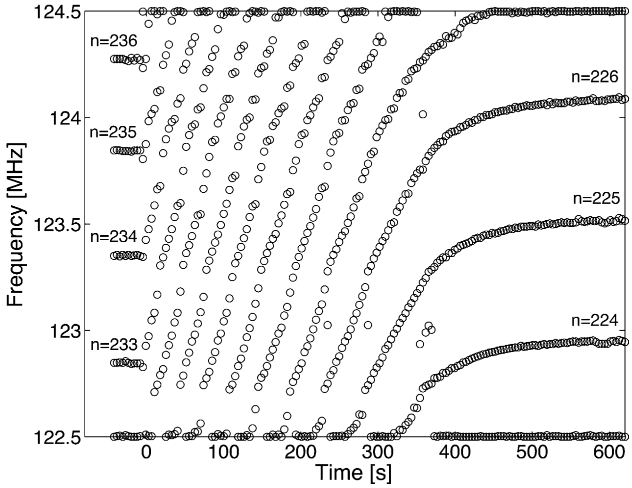

Fig. 9. Interferences mode in the amplitude of the transfer function as a function of time and frequency.

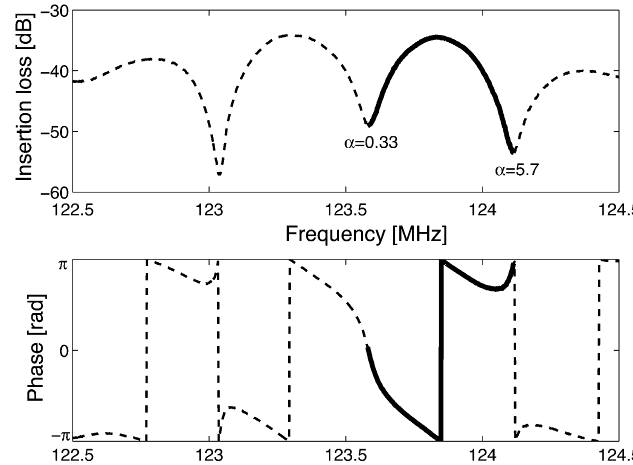

Fig. 11. Evaluation of α at the position of the interference peak.

either by sampling the mode numbers at a constant frequency. Fig. 9 plots the interference peaks versus time and frequency for the etching of the 200 nm thick gold layer; the interference mode numbers n were attributed according to Eqs. (6) and (7) with $V_0 = 4940$ m/s (given by the synchronous frequency of $f_T = 123.5$ MHz times the transducers periodicity λ_T).

The evolution of the velocity in the sensing area with time is representative of the etching rate of the gold layer and is plotted for three different frequencies (123.5, 123.75 and 124 MHz) in Fig. 10. At three different frequencies, the values of velocity should differ as a function of the group velocity. This effect is seen better when the probing frequencies are taken far away from each others and for a strongly dispersive delay line, which is not the case for the experimental device presently used.

At constant frequency, the peaks are spaced by an unit variation of n, therefore the velocity difference measured between two peaks is obtained by differentiation of Eq. (6) with respect to n:

$$\left.\frac{\partial V}{\partial n}\right|_{f_n, V_0} = -\frac{4DV_0^2 f_n}{[(2n+1)V_0 + 2(D-L)f_n]^2}, \tag{33}$$

which gives a variation roughly equals to -40 m/s between two peaks at the three sampling frequencies. From the acoustic velocity variation (4610 m/s for 200 nm gold to 4940 m/s when all the gold is etched) and by assuming that gold has a density of $\rho = 19.3\,\mathrm{g/cm^3}$, we have an evaluation of S_V equals to $-173\,\mathrm{cm^2/g}$. Because the phase loses its periodicity for the thick gold layer, we were not able to determine a value for the phase variation and consequently we have no value for S_ϕ. The Eq. (28) was employed to estimate the value of α at the interference peak; the result is displayed in Fig. 11 that demonstrates a variation of α with the frequency. Around the synchronous frequency, α equals 0.33 and the phase has a periodicity of 2π; but as the frequency is far from the synchronous frequency, α clearly change above the critical value of 1 (in the present case, $\alpha = 5.7$). The consequence is seen in the phase that presents at this point of calculation a positive slope and a periodicity below π.

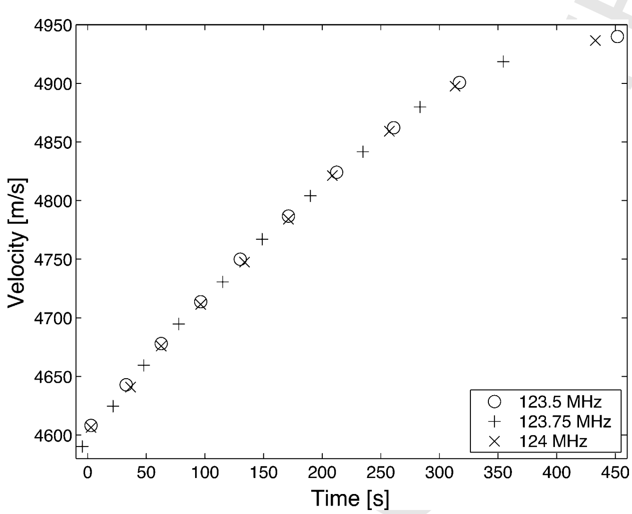

Fig. 10. Evaluation of the acoustic velocity on the sensing are during the etching of the gold as a function of time for different values of frequency.

We applied the same procedure to the thinner gold layer of 50 nm. Fig. 12 shows the transfer function recorded before and after the gold etching; the interference mode number 225 has been followed and give a velocity varying from 4876.5 to 4940 m/s. The resulting velocity sensitivity is $S_V = -96\,\mathrm{cm^2/g}$. This value is lower than the one obtained by etching of the thick gold layer since a thicker layer enhances the sensitivity due to a better entrapment of the acoustic energy in the top guiding layer.

The phase sensitivity S_ϕ could be calculated for frequencies where α remained inferior to the critical value of 1, that is close to the synchronous frequency. The result is plotted versus the frequency in Fig. 13 and compared with the estimated value of S_V while the values of α indicated on the

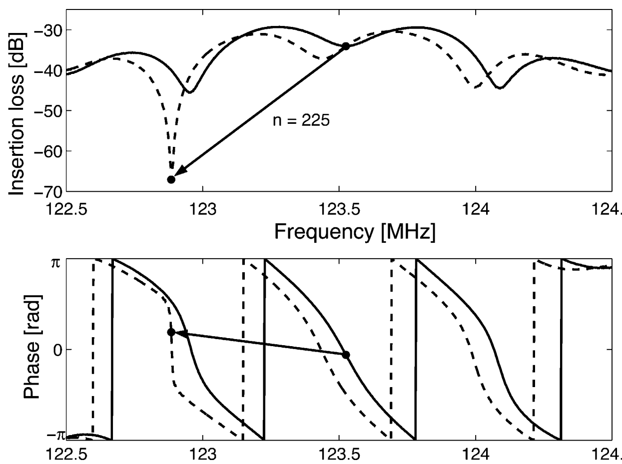

Fig. 12. Transfer function before and after the etching of 50 nm of gold. The arrows indicate the interference mode 225 followed to estimate the velocity sensitivity.

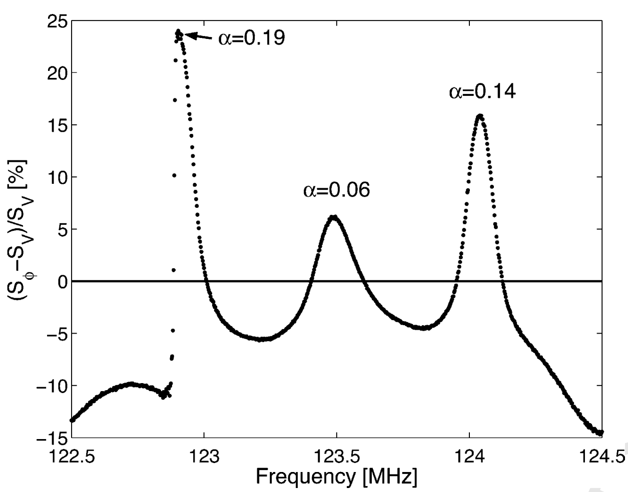

Fig. 13. Phase sensitivity relative to the velocity sensitivity as a function of the frequency and computed from the experimental data obtained by etching 50 nm of gold. Oscillations are attributed to the electromagnetic interferences.

graph have been estimated at the interference peaks thanks to Eq. (29). The graphs shows that the interferences modify the value of the sensitivity as given by Eq. (27). A comparison of the Figs. 6 and 13 shows the correlation between the theoretical modeling of the effects of electromagnetic interferences on the sensitivity of the surface acoustic waveguide sensor and the experimental results.

5. Discussion

Electromagnetic interferences have a clear effect on the transfer function of the acoustic device because of the ripples they cause. The interaction modeled as a constant factor α is specific to each device and must be identified by a careful inspection of the transfer function. The amplitude of the transfer function peak to peak is supposed to be the product between the transfer function of the transducers and the interference, and therefore an evaluation of α is possible if the transfer function of the transducers only is known. However, the experiment shows that α is a function of the frequency and the surface density, indicating that finding its exact value is not straightforward. Only the phase indicates whether α is higher or lower than one.

In term of sensitivity, when $\alpha \geq 1$ the phase has a periodicity P in the range 0–π. We suggest the following correction to the experimental phase sensitivity:

$$S_\phi = \frac{2\pi}{P}\frac{1}{kD}\frac{d\phi}{d\sigma}. \qquad (34)$$

This modification gives a better evaluation of the velocity sensitivity by stretching the phase of the transfer function to 2π. Only the extraction of P is not immediate since it depends upon α. From a physical point of view, α indicates the strength of the electromagnetic wave in comparison with the acoustic wave. For a constant amplitude of the EM wave, a higher α stands for a larger attenuation of the acoustic wave; its precise value is an indication of the actual attenuation of the acoustic wave along the delay line.

The observation of the interference peaks in the experimental part was facilitated by the large velocity change induced by the gold coating. Indeed, 50 nm of gold corresponds to a surface density of 96.5 $\mu g/cm^2$, a relatively large shift in comparison to the targeted (bio)chemical recognition application where molecules films surface density are in the order of hundreds of ng/cm^2 and even lower. The calibration of the sensitivity is best recorded by adding or etching thin layers of materials and that under the operating conditions of the sensor, especially if liquids are involved [16]. In (bio)chemical measurements, the precision on the velocity measurement depends upon the assessments on the initial conditions (i.e. V_0 and n) but also on the induced variation of velocity, which is function of the velocity sensitivity of the waveguide. The evaluation of the mass sensitivity by the frequency variation of an interference peak is identical to a closed loop measurement locked on the interference peak instead on a constant value of the phase. For the detection of a minimum value of the surface density $\Delta\sigma$, the frequency shift of an interference peak must be measured with a precision estimated from Eq. (32):

$$\Delta f_n = \frac{D S_V f_n}{V \tau_g}\Delta\sigma, \qquad (35)$$

that gives $\Delta f_n/\Delta\sigma \simeq -6.5\,cm^2$ Hz/ng in the present case. The detection of a monolayer of proteins, about 400 ng/cm^2, requires to detect a frequency variation of 2.6 kHz, which is compatible with the instrumentation of surface acoustic waveguide sensors.

One benefit of our calculation method resides in the possibility to still measure the acoustic velocity in the sensing area even when the electromagnetic and the acoustic waves

UNCORRECTED PROOF

are strongly interfering, in particular for α greater than one. Strong interferences are unwanted in an experimental set-up because they prevent the correct electrical measurement of the sensor. It must be noticed that for these high values of interference, the electromagnetic wave amplifies the acoustic signal as seen in Fig. 5, which could be of interest for the operation of the device even in conditions where the acoustic signal is weak. Finally, the presented method operates directly on the raw signal of the acoustic device thus avoiding a lost or a modification of the physical information it carries.

6. Conclusion

We have proposed a model for surface acoustic waveguides used as sensors. The model shows the influence of electromagnetic interferences caused by interdigital transducers on the velocity sensitivity in open and closed loop configurations. In both cases, the dimensions of the delay line and the sensing part influence the experimental value of phase or frequency shifts.

The interference peaks in the transfer function offer an unique possibility to access the information about the acoustic phase velocity in the sensing area. The velocity sensitivity was calculated directly from these peaks.

In an open loop configuration and with interferences, the *phase* shift is disturbed and the sensitivity is over- or underestimated to the value of the velocity sensitivity. For strong interferences, the phase has a periodicity lower than 2π that must be considered when normalizing the phase shift to obtain a correct figure of the sensitivity.

In a closed loop configuration and with interferences, the *frequency* shift is not disturbed. The frequency shift is proportional to the sensitivity by the ratio between the length of the sensing area and the distance separating the transducers. In addition, the frequency shift is influenced by the dispersive properties of the waveguide.

The influence of the electromagnetic interferences on the transfer function of a Love mode sensor operating in liquid conditions was presented for a comparison. From the experiment it appears that the interferences are function of both the frequency and the surface density.

For future investigations, an analytical expression of the electromagnetic-acoustic interaction and the parameters acting on it have to be identified in order to reduce the influence or, on the opposite, to enhance the velocity sensitivity of surface acoustic waveguides.

Acknowledgements

The authors are thankful to N. Posthuma for the support with the PECVD tool, to R. De Palma for the help with the gold etching, to C. Bartic for the SU8 walls fabrication, and to A. Campitelli for fruitful discussions. L. Francis is supported by the Fonds pour la Formation à la Recherche dans l'Industrie et dans l'Agriculture (F.R.I.A., Belgium).

References

[1] C. Campbell, Surface Acoustic Wave Devices and Their Signal Processing Applications, Academic Press, San Diego, 1989.
[2] B.A. Auld, Acoustic Fields and Waves in Solids, vol. 2, Wiley, New York, 1973.
[3] G.L. Harding, J. Du, P.R. Dencher, D. Barnett, E. Howe, Love wave acoustic immunosensor operating in liquid, Sens. Actuator A Phys. 61 (1997) 279–286.
[4] E. Gizeli, Design considerations for the acoustic waveguide biosensor, Smart Mater. Struct. 6 (1997) 700–706.
[5] F. Herrmann, M. Weinacht, S. Büttgenbach, Properties of sensors based on shear-horizontal surface acoustic waves in $LiTaO_3/SiO_2$ and Quartz/SiO_2 structures, IEEE Trans. Ultrason. Ferroelectr. Freq. Control 48 (2001) 268–273.
[6] A. Rasmusson, E. Gizeli, Comparison of poly(methylmethacrylate) and Novolak waveguide coatings for an acoustic biosensor, J. App. Phys. 90 (2001) 5911–5914.
[7] G.L. Harding, Mass sensitivity of Love-mode acoustic sensors incorporating silicon dioxide and silicon-oxy-fluoride guiding layers, Sens. Actuator A Phys. 88 (2001) 20–28.
[8] K. Kalantar-Zadeh, W. Wlodarski, Y.Y. Chen, B.N. Fry, K. Galatsis, Novel Love mode surface acoustic wave based immunosensors, Sens. Actuator B-Chem. 91 (2003) 143–147.
[9] Z. Wang, J.D.N. Cheeke, C.K. Jen, Sensitivity analysis for Love mode acoustic gravimetric sensors, Appl. Phys. Lett. 64 (1994) 2940–2942.
[10] B. Jakoby, M. Vellekoop, Properties of Love waves: applications in sensors, Smart Mater. Struct. 6 (1997) 668–679.
[11] G. McHale, F. Martin, M.I. Newton, Mass sensitivity of acoustic wave devices for group and phase velocity measurements, J. Appl. Phys. 92 6 (2002) 3368–3373.
[12] R.M. White, F.W. Voltmer, Direct piezoelectric coupling to surface elastic waves, Appl. Phys. Lett. 7 (1965) 314–316.
[13] G. Feuillard, Y. Janin, F. Teston, L. Tessier, M. Lethiecq, Sensitivities of surface acoustic wave sensors based on fine grain ceramics, in: Instrumentation and Measurement Technology Conference 1996 (IMTC-96), Conference Proceedings 'Quality Measurements: The Indispensable Bridge Between Theory and Reality', vol. 2, IEEE, 1996, pp. 1211–1215.
[14] L.A. Francis, J.-M. Friedt, C. Bartic, A. Campitelli, An SU-8 liquid cell for surface acoustic wave biosensors, Proc. SPIE 5455 (2004) 353–363.
[15] J.L. Vossen, W. Kern, Thin Film Processes, Academic Press, New York, 1978
[16] J.-M. Friedt, L. Francis, K.-H. Choi, F. Frederix, A. Campitelli, Combined atomic force microscope and acoustic wave devices: application to electrodeposition, J. Vac. Sci. Technol. A21 (2003) 1500–1505.

Laurent A. Francis received his BE in materials science with a minor orientation in electrical engineering in 2001 from the Université catholique de Louvain (UCL, Belgium). He is working since then towards the PhD degree at the PCPM unity of UCL in collaboration with IMEC (Belgium) on the study and the realization of acoustic waveguides aiming mainly at biosensing applications.

Jean-Michel Friedt obtained his PhD in engineering from LPMO (CNRS, France) in 2000 after working on scanning probe microscopies and acoustic wave sensors. He spent 3 years at IMEC (Belgium) to complete a study on the combination of acoustic and optical sensors for the characterization of the physical properties of organic layers adsorbed on substrates. He is now a postdoctoral researcher at the LPMO in Besançon (France).

UNCORRECTED PROOF

Patrick Bertrand is Professeur ordinaire at the Université catholique de Louvain (UCL, Belgium). Ingénieur civil physicien, 1971, UCL; PhD, 1976, UCL. Professor at the Facultés Universitaires St. Louis (Belgium). Visiting Professor, University of Houston (USA), 1992. Invited professor at the Institut National de la Recherche Scientifique (INRS) Énergie et Matériaux de Varennes, Université du Québec, Canada, since 1997. President of the Department of Materials Science and Processes, UCL (since 09/1999). Research domain: physical-chemistry of surfaces and interfaces—ion–solid interaction. P. Bertrand has published more than 250 papers in scientific journals with referees, and he has given 40 invited keynote lectures at international conferences.

UNCORRECTED PROOF